Predicting phonon properties and thermal conductivity from anharmonic lattice dynamics calculations and molecular dynamics simulations

J. E. Turney,[1] E. S. Landry,[1] A. J. H. McGaughey,[1,*] and C. H. Amon[1,2]
[1]*Department of Mechanical Engineering, Carnegie Mellon University, Pittsburgh, Pennsylvania 15213, USA*
[2]*Department of Mechanical and Industrial Engineering, University of Toronto, Toronto, Ontario, Canada M5S 3G8*
(Received 13 October 2008; published 19 February 2009)

Two methods for predicting phonon frequencies and relaxation times are presented. The first is based on quasiharmonic and anharmonic lattice dynamics calculations, and the second is based on a combination of quasiharmonic lattice dynamics calculations and molecular dynamics simulations. These phonon properties are then used with the Boltzmann transport equation under the relaxation-time approximation to predict the lattice thermal conductivity. The validity of the low-temperature assumptions made in the lattice dynamics framework are assessed by comparing to thermal conductivities predicted by the Green-Kubo and direct molecular dynamics methods for a test system of Lennard-Jones argon. The predictions of all four methods are in agreement at low temperature (20 K). At temperatures of 40 K (half the Debye temperature of Lennard-Jones argon) and below, the thermal-conductivity predictions from the two methods that use lattice dynamics calculations are within about 30% of those made using the more accurate Green-Kubo and direct molecular dynamics methods. The thermal-conductivity predictions using the lattice dynamics techniques become inaccurate at high temperature (above 40 K) due to the approximations inherent in the lattice dynamics framework. We apply the results to assess the validity of (i) the isotropic approximation in modeling thermal transport and (ii) the common assertion that low-frequency phonons dominate thermal transport. Lastly, we suggest approximations that can be made within the lattice dynamics framework that allow the thermal conductivity of Lennard-Jones argon to be estimated using two orders of magnitude less computing effort than the Green-Kubo or direct molecular dynamics methods.

DOI: 10.1103/PhysRevB.79.064301 PACS number(s): 63.20.kg, 66.70.−f

I. INTRODUCTION

The Fourier law,

$$\mathbf{q} = -\mathbf{k}\nabla T, \tag{1}$$

which describes the conductive heat transfer in a solid or a quiescent fluid, states that the heat flux vector, $\mathbf{q}$, is proportional to the spatial gradient (∇) of temperature, T. The proportionality constant, $\mathbf{k}$, is the thermal conductivity. The thermal conductivity is, in general, a second-rank symmetric tensor. Though formally defined by an empirical relation [Eq. (1)], the thermal conductivity is related to the properties of subcontinuum energy carriers. The energy carriers in solids are electrons and phonons (i.e., lattice vibrations). Electrons are responsible for the majority of heat conduction in metals, while phonons dominate in semiconductors and insulators such as silicon, germanium, and silica-based materials. The heat capacities, velocities, and scattering rates of these carriers are required to predict thermal conductivity.[1]

The transport properties of electrons and phonons can be modified by fabricating materials with nanoscale features. For example, the thermal conductivities of thin films and superlattices are lower than what is predicted from continuum-based theories.[2–6] It has also been found that the thermal conductivity of a solid can be significantly lowered through the addition of appropriately sized nanoparticles.[7–9] The process of designing materials to have specific thermal transport properties is hindered by the complex interactions between the energy carriers and their environment. The design of materials with tailored thermal properties requires tools that can (i) provide detailed information of subcontinuum energy transport (e.g., mode-dependent phonon-scattering rates) and (ii) accurately and efficiently predict thermal conductivity.

In this paper, we present two numerical techniques for predicting phonon properties and thermal conductivity: the Boltzmann transport equation lattice dynamics (BTE-LD) and Boltzmann transport equation molecular dynamics (BTE-MD) methods. The BTE-LD method uses quasiharmonic and anharmonic lattice dynamics (LD) calculations to predict the phonon properties while the BTE-MD method uses quasiharmonic LD calculations and molecular dynamics (MD) simulations. These phonon properties are then related to the lattice thermal conductivity through the Boltzmann transport equation (BTE). We asses the validity of the predictions by providing an in-depth analysis of the low-temperature approximations made in these two methods and by comparing to thermal-conductivity predictions made by the Green-Kubo-MD (GK-MD) and direct-MD methods. The four prediction methods considered here are only valid for materials in which the thermal conductivity is phonon dominated, as they account for energy transported by phonons but not by electrons. In the remainder of this article, the term "thermal conductivity" will be understood to mean thermal conductivity due to phonon transport.

We implement the BTE-LD, BTE-MD, GK-MD, and direct-MD methods to predict the thermal conductivity of crystalline argon at temperatures ranging from 20 to 80 K at 10 K increments. Argon is an insulating face-centered cubic crystal up to its experimentally observed melting temperature of 84 K.[10] We model the interactions between argon atoms with the 12-6 Lennard-Jones (LJ) potential, which gives the energy between a pair of atoms i and j as

$$\phi_{ij}(r_{ij}) = 4\epsilon_{\mathrm{LJ}}\left[\left(\frac{\sigma_{\mathrm{LJ}}}{r_{ij}}\right)^{12} - \left(\frac{\sigma_{\mathrm{LJ}}}{r_{ij}}\right)^{6}\right], \tag{2}$$

where r_{ij} is the distance between the two atoms and the energy and length scales for argon are $\epsilon_{\mathrm{LJ}}=1.67\times10^{-21}$ J and $\sigma_{\mathrm{LJ}}=3.40\times10^{-10}$ m.[11] Argon is chosen because it is an extensively studied material that can be modeled with a simple interatomic potential.[12–15] The methodologies presented herein can also be applied to more complex, technologically relevant insulators and semiconductors, provided that a suitable interatomic potential is available.

A description of the BTE is given in Sec. II, followed by an overview of the quasiharmonic and anharmonic LD calculation techniques in Sec. III. We discuss the BTE-LD and BTE-MD methods in Sec. IV. We then compare the phonon properties predicted by the two BTE-based methods and discuss the validity of the low-temperature approximations made in the LD calculations. We present the results of our thermal-conductivity predictions in Sec. V and identify which phonon modes dominate thermal transport. We also comment on the strengths and weaknesses of each method, addressing computation time, accuracy, and scalability. A description of our implementation of the direct-MD method is provided in the Appendix, while the details of the GK-MD prediction method can be found elsewhere.[14,16]

II. BOLTZMANN TRANSPORT EQUATION

The BTE can be used to track the time evolution of the positions and velocities of a system of particles (e.g., phonons, electrons). For a system of phonons subjected to a temperature gradient, the BTE for a specific phonon mode takes the form[17]

$$\mathbf{v}_g \cdot \nabla T \frac{\partial f_t}{\partial T} = \left(\frac{\partial f_t}{\partial t}\right)_{\mathrm{coll}}, \tag{3}$$

where f_t and $\mathbf{v}_g$ are the phonon distribution function and group-velocity vector and $(\partial f_t/\partial t)_{\mathrm{coll}}$ is the collision term. The left-hand side of Eq. (3) describes a system of noninteracting phonons. On the right-hand side, the collision term accounts for all possible mechanisms of phonon interaction and is generally quite complex. The main challenge in working with the BTE is in specifying and evaluating an expression for the collision term.

The relaxation-time approximation is commonly used to make the BTE tractable.[17] In the relaxation-time approximation, the phonon distribution function and the collision term are written as

$$f_t = f + f', \tag{4}$$

and

$$\left(\frac{\partial f_t}{\partial t}\right)_{\mathrm{coll}} = \frac{-f'}{\tau}, \tag{5}$$

where f is the Bose-Einstein equilibrium distribution function, f' is the fluctuation of the distribution function about equilibrium, and τ is the phonon relaxation time (i.e., the phonon lifetime). The equilibrium distribution function is

$$f = \frac{1}{e^x - 1}, \tag{6}$$

with $x \equiv \hbar\omega/k_B T$, where $\hbar$ is the Planck constant divided by 2π, ω is the phonon frequency, and k_B is the Boltzmann constant. The fluctuations are assumed to be independent of temperature, allowing $\partial f/\partial T$ to be substituted for $\partial f_t/\partial T$ in Eq. (3). Though only phonon-phonon scattering is considered in this study, phonons can also scatter with electrons, system or grain boundaries, and crystal defects such as impurities.[18] The effect of multiple-scattering mechanisms is commonly handled by defining an effective relaxation time with the Matthiessen rule.[17,18]

The net heat flux due to phonon motion is[11]

$$\mathbf{q} = \frac{1}{V}\sum_{\boldsymbol{\kappa}}\sum_{\nu} \hbar\omega \mathbf{v}_g f', \tag{7}$$

where V is the system volume and, together, the two summations run over all phonon modes, which are denoted by wave vector, $\boldsymbol{\kappa}$, and dispersion branch, ν. Combining Eqs. (1) and (7) with Eq. (3) under the relaxation-time approximation yields an expression for the thermal-conductivity tensor,

$$\mathbf{k} = \sum_{\boldsymbol{\kappa}}\sum_{\nu} c_{\mathrm{ph}} \mathbf{v}_g \mathbf{v}_g \tau, \tag{8}$$

where, for a harmonic oscillator, the volumetric phonon specific heat, c_{ph}, is

$$c_{\mathrm{ph}} = \frac{\hbar\omega}{V}\frac{\partial f}{\partial T} = \frac{k_B x^2}{V}\frac{e^x}{[e^x-1]^2}. \tag{9}$$

The thermal conductivity in the classical limit can be obtained by using the classical expressions for the phonon distribution,

$$f^{(C)} = \frac{1}{x}, \tag{10}$$

and specific heat,

$$c_{\mathrm{ph}}^{(C)} = \frac{k_B}{V}, \tag{11}$$

in place of the quantum expressions [Eqs. (6) and (9)].

The argon crystal and its thermal-conductivity tensor are cubically symmetric. The diagonal elements of the thermal-conductivity tensor are therefore equal so that the thermal conductivity is a scalar and can be defined by

$$k = \sum_{\boldsymbol{\kappa}}\sum_{\nu} c_{\mathrm{ph}} v_{g,x}^2 \tau, \tag{12}$$

where $v_{g,x}$ is the x component of the phonon group velocity (i.e., along the [100] direction). Equation (12) is used directly in the BTE-LD and BTE-MD methods (see Sec. IV) in which the mode-dependent phonon properties (c_{ph}, $v_{g,x}$, and τ) are obtained through LD calculations or a combination of LD calculations and MD simulations.

III. LATTICE DYNAMICS CALCULATIONS

A. Quasiharmonic lattice dynamics

Harmonic and quasiharmonic LD calculations can be used to determine the natural frequencies of noninteracting vibrations in a crystal lattice. These vibrational frequencies are the phonon frequencies and lead to the phonon-dispersion relations and density of states. From these phonon frequencies we can determine the phonon group velocities ($\mathbf{v}_g = \partial\omega/\partial\boldsymbol{\kappa}$) and specific heats.

The harmonic LD method makes use of the harmonic approximation and is valid when the atomic motion is small compared to the atomic spacing. In this approximation, the crystal's potential energy is expanded as a Taylor series about the equilibrium atomic positions at zero temperature. The series is then truncated after the second-order term, decoupling the phonon modes. Quasiharmonic LD extends harmonic LD by expanding the potential energy about the average finite-temperature zero-pressure atomic positions. Quasiharmonic LD captures the change in phonon frequencies due to thermal expansion but anharmonic effects due to atomic motion are still excluded.

For a crystal lattice containing N unit cells of n atoms, the quasiharmonic frequencies can be found from the eigenvalue equation

$$\omega^2\left(\begin{matrix}\boldsymbol{\kappa}\\ \nu\end{matrix}\right)\mathbf{e}\left(\begin{matrix}\boldsymbol{\kappa}\\ \nu\end{matrix}\right) = \mathbf{D}(\boldsymbol{\kappa})\mathbf{e}\left(\begin{matrix}\boldsymbol{\kappa}\\ \nu\end{matrix}\right), \tag{13}$$

where, for each $\boldsymbol{\kappa}$ and ν, the eigenvalues, $\omega^2(\begin{smallmatrix}\boldsymbol{\kappa}\\ \nu\end{smallmatrix})$, are the squares of the quasiharmonic phonon frequencies with associated eigenvector (mode shape) $\mathbf{e}(\begin{smallmatrix}\boldsymbol{\kappa}\\ \nu\end{smallmatrix})$. The dynamical matrix, $\mathbf{D}(\boldsymbol{\kappa})$, has dimension $3n \times 3n$ with elements defined by

$$D_{3(b-1)+\alpha,3(b'-1)+\alpha'}(\boldsymbol{\kappa}) = \frac{1}{\sqrt{m_b m_{b'}}}\sum_{l'}^{N} \left.\frac{\partial^2\Phi}{\partial r_\alpha\left(\begin{matrix}0\\ b\end{matrix}\right)\partial r_{\alpha'}\left(\begin{matrix}l'\\ b'\end{matrix}\right)}\right|_o \times \exp\left\{i\boldsymbol{\kappa}\cdot\left[\mathbf{r}\left(\begin{matrix}l'\\ b'\end{matrix}\right) - \mathbf{r}\left(\begin{matrix}0\\ b\end{matrix}\right)\right]\right\}, \tag{14}$$

where b and α index over the atoms in the unit cell and Cartesian coordinates, Φ is the crystal potential energy [$\Phi = \frac{1}{2}\Sigma_i\Sigma_j\phi_{ij}(r_{ij})$ for a pair potential], $\mathbf{r}(\begin{smallmatrix}l\\ b\end{smallmatrix})$ is the average position vector for the bth atom in the lth unit cell with $r_\alpha(\begin{smallmatrix}l\\ b\end{smallmatrix})$ its α component, and m is the atomic mass (6.63×10^{-26} kg for argon). Details of the derivation of Eqs. (13) and (14) are given elsewhere.[19,20]

B. Anharmonic lattice dynamics

In anharmonic LD, phonon interactions are reintroduced as a perturbation to the quasiharmonic solution. Anharmonic LD calculations can be used to find the mode-dependent frequency shift, Δ, and linewidth, Γ, from[21,22]

$$\Delta\left(\begin{matrix}\boldsymbol{\kappa}\\ \nu\end{matrix}\right) = \frac{\hbar}{16N}\sum_{\boldsymbol{\kappa}',\nu'}^{N,3n}\sum_{\boldsymbol{\kappa}'',\nu''}^{N,3n}\left|\Phi\left(\begin{matrix}\boldsymbol{\kappa} & \boldsymbol{\kappa}' & \boldsymbol{\kappa}''\\ \nu & \nu' & \nu''\end{matrix}\right)\right|^2\left\{\left[f\left(\begin{matrix}\boldsymbol{\kappa}'\\ \nu'\end{matrix}\right)+f\left(\begin{matrix}\boldsymbol{\kappa}''\\ \nu''\end{matrix}\right)+1\right]\left[\left(\omega\left(\begin{matrix}\boldsymbol{\kappa}\\ \nu\end{matrix}\right)-\omega\left(\begin{matrix}\boldsymbol{\kappa}'\\ \nu'\end{matrix}\right)-\omega\left(\begin{matrix}\boldsymbol{\kappa}''\\ \nu''\end{matrix}\right)\right)_p^{-1} - \left(\omega\left(\begin{matrix}\boldsymbol{\kappa}\\ \nu\end{matrix}\right)+\omega\left(\begin{matrix}\boldsymbol{\kappa}'\\ \nu'\end{matrix}\right)+\omega\left(\begin{matrix}\boldsymbol{\kappa}''\\ \nu''\end{matrix}\right)\right)_p^{-1}\right] + \left[f\left(\begin{matrix}\boldsymbol{\kappa}'\\ \nu'\end{matrix}\right)-f\left(\begin{matrix}\boldsymbol{\kappa}''\\ \nu''\end{matrix}\right)\right]\left[\left(\omega\left(\begin{matrix}\boldsymbol{\kappa}\\ \nu\end{matrix}\right)+\omega\left(\begin{matrix}\boldsymbol{\kappa}'\\ \nu'\end{matrix}\right)-\omega\left(\begin{matrix}\boldsymbol{\kappa}''\\ \nu''\end{matrix}\right)\right)_p^{-1} - \left(\omega\left(\begin{matrix}\boldsymbol{\kappa}\\ \nu\end{matrix}\right)-\omega\left(\begin{matrix}\boldsymbol{\kappa}'\\ \nu'\end{matrix}\right)+\omega\left(\begin{matrix}\boldsymbol{\kappa}''\\ \nu''\end{matrix}\right)\right)_p^{-1}\right]\right\} - \frac{\hbar}{8N}\sum_{\boldsymbol{\kappa}',\nu'}^{N,3n}\sum_{\nu''}^{3n}\Phi\left(\begin{matrix}-\boldsymbol{\kappa} & \boldsymbol{\kappa} & 0\\ \nu & \nu' & \nu''\end{matrix}\right)\Phi\left(\begin{matrix}-\boldsymbol{\kappa}' & \boldsymbol{\kappa}' & 0\\ \nu & \nu' & \nu''\end{matrix}\right)\left[2f\left(\begin{matrix}\boldsymbol{\kappa}'\\ \nu'\end{matrix}\right)+1\right]\left[\omega\left(\begin{matrix}\boldsymbol{\kappa}''\\ \nu''\end{matrix}\right)\right]_p^{-1} + \frac{\hbar}{8N}\sum_{\boldsymbol{\kappa}',\nu'}^{N,3n}\Phi\left(\begin{matrix}\boldsymbol{\kappa} & \boldsymbol{\kappa}' & -\boldsymbol{\kappa} & -\boldsymbol{\kappa}'\\ \nu & \nu' & \nu & \nu'\end{matrix}\right)\left[2f\left(\begin{matrix}\boldsymbol{\kappa}'\\ \nu'\end{matrix}\right)+1\right], \tag{15}$$

$$\Gamma\left(\begin{matrix}\boldsymbol{\kappa}\\ \nu\end{matrix}\right) = \frac{\pi\hbar}{16N}\sum_{\boldsymbol{\kappa}',\nu'}^{N,3n}\sum_{\boldsymbol{\kappa}'',\nu''}^{N,3n}\left|\Phi\left(\begin{matrix}\boldsymbol{\kappa} & \boldsymbol{\kappa}' & \boldsymbol{\kappa}''\\ \nu & \nu' & \nu''\end{matrix}\right)\right|^2\left\{\left[f\left(\begin{matrix}\boldsymbol{\kappa}'\\ \nu'\end{matrix}\right)+f\left(\begin{matrix}\boldsymbol{\kappa}''\\ \nu''\end{matrix}\right)+1\right]\left[\delta\left(\omega\left(\begin{matrix}\boldsymbol{\kappa}\\ \nu\end{matrix}\right)-\omega\left(\begin{matrix}\boldsymbol{\kappa}'\\ \nu'\end{matrix}\right)-\omega\left(\begin{matrix}\boldsymbol{\kappa}''\\ \nu''\end{matrix}\right)\right)\right] + \left[f\left(\begin{matrix}\boldsymbol{\kappa}'\\ \nu'\end{matrix}\right)-f\left(\begin{matrix}\boldsymbol{\kappa}''\\ \nu''\end{matrix}\right)\right] \times\left[\delta\left(\omega\left(\begin{matrix}\boldsymbol{\kappa}\\ \nu\end{matrix}\right)+\omega\left(\begin{matrix}\boldsymbol{\kappa}'\\ \nu'\end{matrix}\right)-\omega\left(\begin{matrix}\boldsymbol{\kappa}''\\ \nu''\end{matrix}\right)\right)-\delta\left(\omega\left(\begin{matrix}\boldsymbol{\kappa}\\ \nu\end{matrix}\right)-\omega\left(\begin{matrix}\boldsymbol{\kappa}'\\ \nu'\end{matrix}\right)+\omega\left(\begin{matrix}\boldsymbol{\kappa}''\\ \nu''\end{matrix}\right)\right)\right]\right\}. \tag{16}$$

Equations (15) and (16) can be computed in the classical limit by substituting $f^{(C)}-1/2$ [see Eq. (10)] in place of f. The Cauchy principal value, $()_p$, and Dirac delta function, $\delta()$, are defined for a function $g(x)$ by

$$\int_a^b [g(x)]_p dx = \lim_{\gamma\to 0^+}\left[\int_a^{c-\gamma} g(x)dx + \int_{c+\gamma}^b g(x)dx\right] \quad (17)$$

and

$$\int_{-\infty}^{\infty} g(x)\delta(x-a)dx = g(a). \quad (18)$$

The term $\Phi\left(\begin{smallmatrix}\boldsymbol{\kappa}_1 & \boldsymbol{\kappa}_2 & \cdots & \boldsymbol{\kappa}_i\\ \nu_1 & \nu_2 & \cdots & \nu_i\end{smallmatrix}\right)$ contains the ith-order derivative of the potential energy evaluated at the average atomic positions and is defined as

$$\Phi\begin{pmatrix}\boldsymbol{\kappa}_1 & \boldsymbol{\kappa}_2 & \cdots & \boldsymbol{\kappa}_i\\ \nu_1 & \nu_2 & \cdots & \nu_i\end{pmatrix} = \sum_{\alpha_1,b_1}^{3,n}\sum_{\alpha_2,b_2,l_2}^{3,n,N}\cdots\sum_{\alpha_1,b_i,l_i}^{3,n,N}\delta_{(\boldsymbol{\kappa}_1+\boldsymbol{\kappa}_2+\cdots+\boldsymbol{\kappa}_i),\mathbf{K}}\left.\frac{\partial^i\Phi}{\partial r_{\alpha_1}\begin{pmatrix}0\\ b_1\end{pmatrix}\partial r_{\alpha_2}\begin{pmatrix}l_2\\ b_2\end{pmatrix}\cdots\partial r_{\alpha_i}\begin{pmatrix}l_i\\ b_i\end{pmatrix}}\right|_o$$
$$\times\frac{\tilde{e}\begin{pmatrix}\boldsymbol{\kappa}_1 & b_1\\ \nu_1 & \alpha_1\end{pmatrix}\tilde{e}\begin{pmatrix}\boldsymbol{\kappa}_2 & b_2\\ \nu_2 & \alpha_2\end{pmatrix}\cdots\tilde{e}\begin{pmatrix}\boldsymbol{\kappa}_i & b_i\\ \nu_i & \alpha_i\end{pmatrix}}{\sqrt{m_{b_1}\omega\begin{pmatrix}\boldsymbol{\kappa}_1\\ \nu_1\end{pmatrix}m_{b_2}\omega\begin{pmatrix}\boldsymbol{\kappa}_2\\ \nu_2\end{pmatrix}\cdots m_{b_i}\omega\begin{pmatrix}\boldsymbol{\kappa}_i\\ \nu_i\end{pmatrix}}}\exp\left[i\boldsymbol{\kappa}_2\cdot\mathbf{r}\begin{pmatrix}l_2\\ 0\end{pmatrix}\right]\cdots\exp\left[i\boldsymbol{\kappa}_i\cdot\mathbf{r}\begin{pmatrix}l_i\\ 0\end{pmatrix}\right], \quad (19)$$

where

$$\tilde{e}\begin{pmatrix}\boldsymbol{\kappa} & b\\ \nu & \alpha\end{pmatrix} = e\begin{pmatrix}\boldsymbol{\kappa} & b\\ \nu & \alpha\end{pmatrix}\exp\left[i\boldsymbol{\kappa}\cdot\mathbf{r}\begin{pmatrix}0\\ b\end{pmatrix}\right], \quad (20)$$

with $e\left(\begin{smallmatrix}\boldsymbol{\kappa} & b\\ \nu & \alpha\end{smallmatrix}\right)$ being the eigenvector component associated with atom b and the α direction. The Kronecker delta, $\delta_{(\boldsymbol{\kappa}_1+\boldsymbol{\kappa}_2+\cdots+\boldsymbol{\kappa}_i),\mathbf{K}}$, is one if the sum of the wave vectors is a reciprocal-lattice vector, $\mathbf{K}$, and zero otherwise.

The frequency shift and linewidth are the second-order anharmonic corrections to the quasiharmonic frequencies. The corrections include contributions from three- and four-phonon processes, which depend upon the third- and fourth-order derivatives of the potential energy. The delta functions impose energy conservation and can be interpreted as decay channels whereby the phonon of interest splits into two phonons $\{\delta[\omega(\boldsymbol{\kappa}_\nu)-\omega(\boldsymbol{\kappa}'_{\nu'})-\omega(\boldsymbol{\kappa}''_{\nu''})]\}$ or combines with another phonon to produce a third $\{\delta[\omega(\boldsymbol{\kappa}_\nu)\pm\omega(\boldsymbol{\kappa}'_{\nu'})\mp\omega(\boldsymbol{\kappa}''_{\nu''})]\}$. The Kronecker delta enforces conservation of quasimomentum up to a reciprocal-lattice vector. Phonon processes where $\mathbf{K}=0$ are normal processes while for Umklapp processes $\mathbf{K}\neq 0$.

If the frequency shift and linewidth are small compared to the quasiharmonic frequency, the time-dependent normal-mode coordinate, $Q(\boldsymbol{\kappa}_\nu)$, can be written as[23]

$$Q\begin{pmatrix}\boldsymbol{\kappa}\\ \nu\end{pmatrix} = Q_o\begin{pmatrix}\boldsymbol{\kappa}\\ \nu\end{pmatrix}\exp\left\{-i\left[\omega\begin{pmatrix}\boldsymbol{\kappa}\\ \nu\end{pmatrix}+\Delta\begin{pmatrix}\boldsymbol{\kappa}\\ \nu\end{pmatrix}-i\Gamma\begin{pmatrix}\boldsymbol{\kappa}\\ \nu\end{pmatrix}\right]t\right\}, \quad (21)$$

where $Q_o(\boldsymbol{\kappa}_\nu)$ is a mode-dependent constant and t is time. From Eq. (21), it can be seen that $\Delta(\boldsymbol{\kappa}_\nu)$ is the shift in the quasiharmonic vibrational frequency while $\Gamma(\boldsymbol{\kappa}_\nu)$ is a decay rate. The anharmonic frequency, $\omega_A(\boldsymbol{\kappa}_\nu)$, is

$$\omega_A\begin{pmatrix}\boldsymbol{\kappa}\\ \nu\end{pmatrix} = \omega\begin{pmatrix}\boldsymbol{\kappa}\\ \nu\end{pmatrix}+\Delta\begin{pmatrix}\boldsymbol{\kappa}\\ \nu\end{pmatrix}, \quad (22)$$

and the relaxation time is the mean lifetime of the squared normal-mode coordinate[23] [see Eq. (29)],

$$\tau\begin{pmatrix}\boldsymbol{\kappa}\\ \nu\end{pmatrix} = \frac{1}{2\Gamma\begin{pmatrix}\boldsymbol{\kappa}\\ \nu\end{pmatrix}}. \quad (23)$$

With these phonon properties, we can predict the thermal conductivity from Eq. (12).

IV. BOLTZMANN TRANSPORT EQUATION-BASED METHODS

A. Overview

The BTE-LD and BTE-MD methods are similar in that the thermal conductivity is predicted from Eq. (12). These methods differ, though, in how the phonon properties are obtained. In the BTE-LD method, the phonon properties are found with quasiharmonic and anharmonic LD calculations. In the BTE-MD method, the phonon properties are determined through a combination of quasiharmonic LD calculations and MD simulations.

Several authors have combined the BTE with quasiharmonic and anharmonic LD calculations to predict thermal conductivity. Using the same basic theory presented in Secs. II and III, Ladd *et al.*[23] computed the low-temperature thermal conductivity for an inverse twelfth-power potential and found good agreement with results from the GK-MD

method. Omini and Sparavigna[24–26] developed an iterative method to solve an inelastic form of the BTE (the relaxation-time approximation assumes elastic scattering) and applied it to predict the thermal conductivity of argon, krypton, silicon, and germanium. In their method, Omini and Sparavigna used quasiharmonic LD calculations to provide input for predicting three-phonon-scattering probabilities using terms similar to those in Eq. (16). Broido and co-workers[27–29] applied the iterative method of Omini and Sparavigna to study the thermal conductivity of superlattices, bulk silicon, and bulk germanium.

The BTE-MD method was first proposed by Ladd *et al.*[23] and extended by McGaughey and Kaviany.[14,30] McGaughey and Kaviany applied the BTE-MD method to predict the thermal conductivity of LJ argon under the isotropic approximation. Others have since used the method to predict the thermal conductivity of silicon, also under the isotropic approximation.[31,32] The validity of the isotropic assumption for LJ argon will be discussed in Sec. IV B.

B. BTE-LD method

In the BTE-LD method, the thermal conductivity is predicted using phonon information as input to the BTE under the relaxation-time approximation. The phonon information is found through the quasiharmonic and anharmonic LD calculations described in Sec. III. To best compare with the results of the MD prediction methods, the BTE-LD thermal-conductivity predictions and all other calculations presented here are made in the classical limit unless otherwise noted. For our calculations, we consider the four-atom conventional unit cell arrayed on a simple-cubic lattice. The quasiharmonic phonon frequencies and polarization vectors are computed with quasiharmonic LD on a $N_1 \times N_2 \times N_3$ grid of wave vectors, making the total number of unit cells, N, equal to $N_1 N_2 N_3$. The quasiharmonic frequencies and polarization vectors are then used as inputs to an anharmonic LD calculation, the results of which are used to determine the anharmonic frequency and relaxation time of each phonon mode. The lattice parameters, a, used are those from MD simulations reported by McGaughey[16] and the cutoff radius is set to $2.5\sigma_{\mathrm{LJ}}$ for the quasiharmonic calculations and $1.5\sigma_{\mathrm{LJ}}$ (nearest neighbors) for the anharmonic LD calculations. Using the smaller cutoff in the anharmonic calculation changes the calculated frequency shifts and linewidths by less than 7% and the thermal conductivity by less than 2%, while reducing the computational effort by one third. We further reduce the computational effort required in the anharmonic LD calculations by considering crystal symmetry. To obtain the dynamics of all phonons it is sufficient to only consider the irreducible Brillouin zone, whose volume is 1/48th of that of the full first Brillouin zone for simple, face-centered, and body-centered cubic crystals.[17]

There are three major challenges associated with implementing the BTE-LD method. We have developed procedures to overcome each of these challenges. The first challenge is to compute the x component of the group velocity. This velocity is found at each grid point by a finite difference of the quasiharmonic frequencies, which can be evaluated at arbitrary wave vectors in order to compute an accurate numerical derivative. Since the phonons used for the finite difference are similar to each other (i.e., nearly equal frequencies, polarizations, and wave vectors), we expect their frequency shifts to be approximately equal. The group velocities based on the quasiharmonic frequencies can thus be converted to anharmonic group velocities by scaling by ω_A/ω.

The second challenge is to evaluate the Cauchy principal value and Dirac delta function [see Eqs. (17) and (18)]. These functions are defined in terms of integrals, but Eqs. (15) and (16) involve summations over a discrete set of wave vectors. One common way to address this challenge is to approximate the principal value and delta function by[22,23]

$$\frac{1}{(\omega)_p} \approx \frac{\omega}{\omega^2 + \epsilon^2} \tag{24}$$

and

$$\delta(\omega) \approx \frac{1}{\pi} \frac{\epsilon}{\omega^2 + \epsilon^2}, \tag{25}$$

where ϵ is a small positive number that removes the discontinuity from the principal value and broadens the delta function. The proper choice of ϵ is vital. If ϵ is too large, the details of the phonon-phonon interactions will be washed out. If ϵ is too small, there will not be enough interacting phonons to yield meaningful results. We use Eqs. (24) and (25) in our anharmonic LD calculations and let

$$\epsilon = \Gamma\begin{pmatrix} \boldsymbol{\kappa} \\ \nu \end{pmatrix} + \Gamma\begin{pmatrix} \boldsymbol{\kappa}' \\ \nu' \end{pmatrix} + \Gamma\begin{pmatrix} \boldsymbol{\kappa}'' \\ \nu'' \end{pmatrix} \tag{26}$$

for all three-phonon processes. We arrive at Eq. (26) by using the corrected phonon frequencies $(\omega_A \pm i\Gamma)$ in place of the quasiharmonic frequencies (ω) in Eqs. (15), (16), and (19). This substitution couples the frequency shift and linewidth equations for all the phonon modes. We solve these equations by providing an initial guess for the frequency shift and linewidth and iterating until self-consistency is achieved. All predictions obtained from the BTE-LD calculations are the result of five iterations. The difference between the thermal conductivities of the last two iterations is always less than 0.5%.

The third challenge associated with the BTE-LD method is to account for the effect of the resolution of the wave vector grid (i.e., N, the number of unit cells considered). The frequency shift and linewidth are found to be nearly independent of the number of wave vectors but the thermal conductivity increases with increasing N. This dependence is due to summing over a finite number of wave vectors in Eq. (12). The three zone-center (Γ-point/$\boldsymbol{\kappa}=0$) acoustic phonons are related to bulk translation, and thus do not contribute to the thermal conductivity. Excluding these phonons subtracts a reciprocal space volume of $3 \times 8\pi^3/a^3 N$ from the first Brillouin zone. Using a denser grid of wave vectors reduces the amount of the first Brillouin zone excluded from the summation. We find that an extrapolation technique works well for removing the predicted thermal conductivity's dependence upon the wave vector grid. We take lattices where $N_1 = N_2$

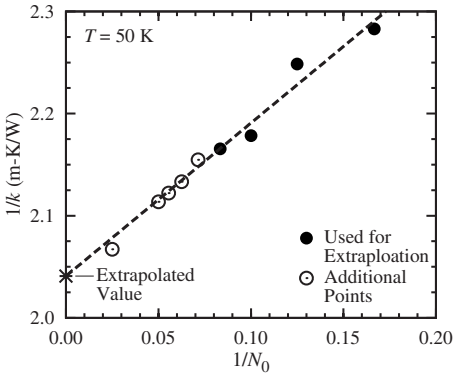

FIG. 1. $1/k$ versus $1/N_0$ and linear fit for extrapolation from BTE-LD calculations at a temperature of 50 K. The line is fit to the four rightmost (filled) circles only.

$=N_3=N_0$ and plot $1/k$ versus $1/N_0$, as shown in Fig. 1. A linear fit to the data yields the inverse of the thermal conductivity as the vertical intercept. Performing the extrapolation with any four of the points shown in Fig. 1 changes the thermal conductivity by at most $\pm 1.5\%$. The thermal-conductivity values reported in Sec. V are extrapolated from the linear fit to $N_0=6$, 8, 10, and 12.

C. BTE-MD method

In the BTE-MD method, MD simulations are used to determine the anharmonic phonon frequencies and relaxation times. In a MD simulation, models for the interactions between atoms (i.e., interatomic potentials) are used with Newton's laws of motion to predict the positions and velocities of the atoms over time. These trajectories can then be used to extract relevant statistics about material behavior, such as specific heat and thermal conductivity. The MD simulation method is a classical method, meaning that the results are only valid when quantum effects can be neglected. Thermal-conductivity predictions from MD simulations can provide reasonable agreement with experiment down to about one tenth of the Debye temperature,[33] T_{Debye}, which is found from MD simulation (experiment) to be 81 K (85 K) for argon.[11,16]

The first step in the BTE-MD method is to determine the noninteracting phonon frequencies and polarization vectors from a quasiharmonic LD calculation (see Sec. III A). Molecular dynamics simulations are then used to calculate the time-dependent normal-mode coordinates, $Q\left(\begin{smallmatrix}\boldsymbol{\kappa}\\ \nu\end{smallmatrix}\right)$, from the expression

$$Q\left(\begin{matrix}\boldsymbol{\kappa}\\ \nu\end{matrix}\right) = \sum_j \left[\frac{m_j}{nN}\right]^{1/2} \exp[-i\boldsymbol{\kappa}\cdot\mathbf{r}_{j,o}]\mathbf{e}\left(\begin{matrix}-\boldsymbol{\kappa}\\ \nu\end{matrix}\right)\cdot[\mathbf{r}_j-\mathbf{r}_{j,o}], \tag{27}$$

where nN is the total number of atoms and $\mathbf{r}_{j,o}$ is the equilibrium position of the jth atom.

The time-dependent energy of each quasiharmonic oscillator is then found from

$$E_{\boldsymbol{\kappa},\nu}(t) = \frac{\omega^2\left(\begin{matrix}\boldsymbol{\kappa}\\ \nu\end{matrix}\right)Q^*\left(\begin{matrix}\boldsymbol{\kappa}\\ \nu\end{matrix}\right)Q\left(\begin{matrix}\boldsymbol{\kappa}\\ \nu\end{matrix}\right)}{2} + \frac{\dot{Q}^*\left(\begin{matrix}\boldsymbol{\kappa}\\ \nu\end{matrix}\right)\dot{Q}\left(\begin{matrix}\boldsymbol{\kappa}\\ \nu\end{matrix}\right)}{2}, \tag{28}$$

where the first and second terms on the right-hand side are the potential and kinetic energies. Using Eq. (21) we find that the autocorrelation of the phonon energy [Eq. (28)] is described by

$$\exp\left[-t/\tau\left(\begin{matrix}\boldsymbol{\kappa}\\ \nu\end{matrix}\right)\right] = \frac{\langle E_{\boldsymbol{\kappa},\nu}(t)E_{\boldsymbol{\kappa},\nu}(0)\rangle}{\langle E_{\boldsymbol{\kappa},\nu}(0)E_{\boldsymbol{\kappa},\nu}(0)\rangle}, \tag{29}$$

where the angle brackets denote an ensemble average, which for an ergodic system is equivalent to a time average. We fit an exponential decay to the normalized energy autocorrelation to extract the relaxation time. The autocorrelation of the phonon potential energy gives a decaying function that oscillates with a period that is π divided by the anharmonic phonon frequency. We compute the phonon group velocities in the same way we do for the BTE-LD method, scaling quasiharmonic velocities by ω_A/ω to get anharmonic velocities. The phonon specific heats are computed with the classical expression [Eq. (11)]. While Eq. (11) is an approximation for an anharmonic system, it has been found to be accurate to within 6% at temperatures of 50 K and below.[14]

For our MD simulations, we use the velocity Verlet integration algorithm with a time step of 4.3 fs. The lattice parameters used are those from MD simulations reported by McGaughey[16] and a radius of $2.5\sigma_{\text{LJ}}$ is used for the interatomic potential cutoff. We allow the system to equilibrate for a period of 1×10^5 time steps after which we compute the normal-mode coordinate and its derivative every fifth time step for an additional 2×10^6 time steps. The anharmonic frequency and lifetime are computed for every phonon in the irreducible Brillouin zone and averaged over five independent simulations. Like in the BTE-LD method, the thermal conductivity predicted from the BTE-MD method is found to depend on the number of wave vectors. In the same manner as the BTE-LD method, we remove this dependence by extrapolating to an infinite number of wave vectors using $N_0\times N_0\times N_0$ lattices with $N_0=4$, 6, 8, and 10.

D. Comparison and validation of the Boltzmann transport equation-based methods

As discussed in Sec. III, for the quasiharmonic and anharmonic LD calculations to be valid, (i) the atomic displacements must be small compared to the atomic spacing and (ii) the frequency shift and linewidth must be small compared to the quasiharmonic frequencies. The first condition affects both the BTE-LD and BTE-MD methods since they both rely on quasiharmonic LD calculations. The second condition also applies to both methods as the BTE-LD method uses anharmonic LD calculations directly and the BTE-MD method requires the phonon modes to be well described by Eq. (21). We expect the BTE-MD method to be more accurate than the BTE-LD method at all temperatures because the MD simulations include the full anharmonicity of the interatomic potential while the anharmonic LD calculation only considers up to four-phonon processes. The BTE-based

TABLE I. Root mean-square displacements scaled by the nearest-neighbor distance from the BTE-LD and BTE-MD methods. The data in the rightmost column are RMS displacements found directly from a time average of the atomic positions in MD simulations (Ref. 16).

T (K)	$\frac{\langle u^2_{\mathrm{LD}}\rangle^{1/2}}{a/\sqrt{2}}$	$\frac{\langle u^2_{\mathrm{MD}}\rangle^{1/2}}{a/\sqrt{2}}$	$\frac{\langle u^2(\mathbf{r})\rangle^{1/2}}{a/\sqrt{2}}$
20	0.047	0.048	0.048
30	0.059	0.060	0.065
40	0.070	0.072	0.081
50	0.080	0.083	0.10
60	0.091	0.096	0.12
70	0.10	0.11	0.15
80	0.11	0.13	0.18

methods should converge at low temperature where the approximations made in the LD techniques are accurate.

Tabulated in Table I are the classical BTE-LD- and BTE-MD-predicted root-mean-square (RMS) displacements,[34]

$$\langle u^2\rangle^{1/2} = \left[\frac{\hbar}{nN}\sum_{\alpha,b}^{3,n}\sum_{\boldsymbol{\kappa},\nu}^{N,3n} f\begin{pmatrix}\boldsymbol{\kappa}\\ \nu\end{pmatrix}\frac{e\begin{pmatrix}\boldsymbol{\kappa} & b\\ \nu & \alpha\end{pmatrix}e^*\begin{pmatrix}\boldsymbol{\kappa} & b\\ \nu & \alpha\end{pmatrix}}{m_b\omega_A\begin{pmatrix}\boldsymbol{\kappa}\\ \nu\end{pmatrix}}\right]^{1/2}, \tag{30}$$

scaled by the nearest-neighbor distance, $a/\sqrt{2}$. Also tabulated in Table I are the scaled RMS displacements, $\langle u^2(\mathbf{r})\rangle^{1/2}/(a/\sqrt{2})$, found directly from the time average of the atomic positions in a MD simulation.[16] At a temperature of 20 K the atomic displacements from the BTE-based methods are in excellent agreement with the formally exact value obtained from MD simulation. At a temperature of 40 K the BTE-LD-predicted RMS displacement is 14% smaller than the value obtained directly from MD and becomes increasingly inaccurate at higher temperatures. The RMS displacements calculated from the BTE-MD method are more accurate than the BTE-LD-predicted values but also lose accuracy at higher temperatures.

The frequency shifts and inverse lifetimes at temperatures of 20 and 50 K are plotted versus wave vector in the [100] direction in Figs. 2(a)–2(d). For the BTE-MD method, predictions are made using (i) the full LJ potential and (ii) a Taylor-series expansion of the LJ potential truncated after the fourth-order term. The frequency shifts [Figs. 2(a) and 2(b)] and inverse lifetimes [Figs. 2(c) and 2(d)] computed with the BTE-LD method and the BTE-MD method (using the full and truncated LJ potential) are in good agreement at a temperature of 20 K where the low-temperature approximations are valid (see Table I). The results from the BTE-MD method using the full LJ potential at both temperatures are in good agreement with the frequency shifts and relaxation times found by McGaughey and Kaviany.[14,30]

At a temperature of 50 K the fifth- and higher-order terms in the potential-energy expansion become important. The effect of these terms is evident in the clear differences between the results from the BTE-MD calculations using the full LJ potential and the truncated potential (circles and triangles). We take the frequency shifts and lifetimes calculated using

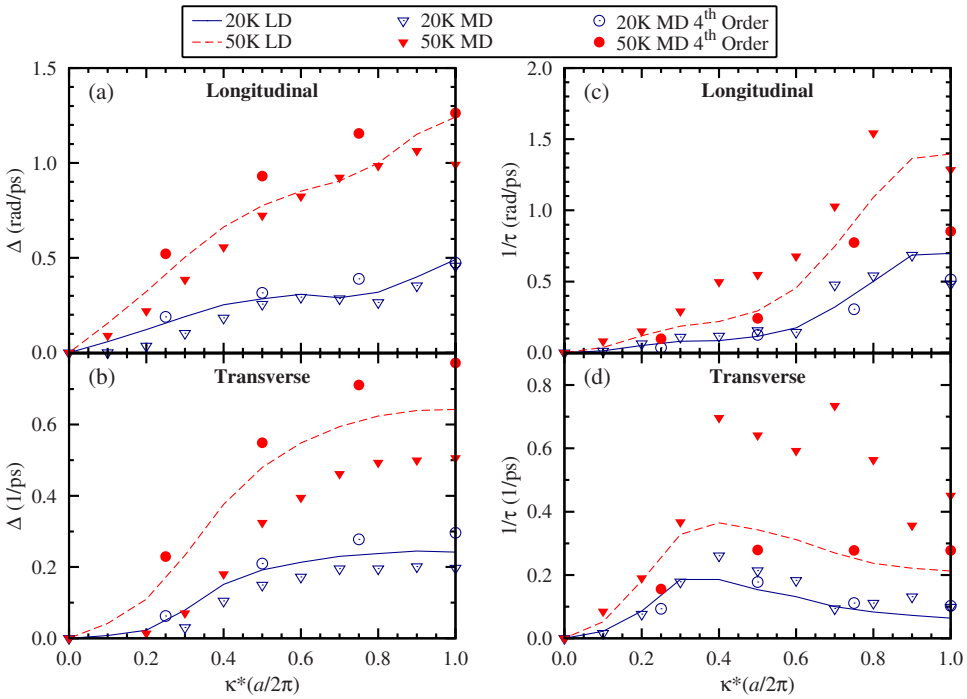

FIG. 2. (Color online) Frequency shift (Δ) and inverse of the lifetime ($1/\tau$) at temperatures of 20 and 50 K versus reduced wave vector for the longitudinal and transverse dispersion branches in the [100] direction. The MD data is found using (i) the full LJ potential and (ii) the LJ potential truncated after the fourth-order term in the Taylor-series expansion. While the results from the LD calculations are discrete, we plot the data as lines for clarity.

TABLE II. Root mean-square anharmonic frequency shifts and linewidths ($\Gamma = 1/2\tau$) normalized by the quasiharmonic frequencies from the BTE-LD and BTE-MD methods.

T (K)	$\langle \frac{\Delta_{LD}^2}{\omega^2} \rangle^{1/2}$	$\langle \frac{\Delta_{MD}^2}{\omega^2} \rangle^{1/2}$	$\langle \frac{\Gamma_{LD}^2}{\omega^2} \rangle^{1/2}$	$\langle \frac{\Gamma_{MD}^2}{\omega^2} \rangle^{1/2}$
20	0.029	0.023	0.013	0.014
30	0.048	0.039	0.020	0.025
40	0.069	0.056	0.028	0.037
50	0.094	0.074	0.035	0.054
60	0.13	0.096	0.043	0.078
70	0.16	0.12	0.051	0.11
80	0.22	0.15	0.059	0.16

the BTE-MD method with the full LJ potential to be the most accurate. The truncated potential is less anharmonic than the full potential, resulting in longer phonon lifetimes. The results from the BTE-LD method (in which the potential energy is truncated after the fourth-order term) are generally in good agreement with the results from the BTE-MD method using the truncated potential. The discrepancies between these two methods can be attributed to the fact that the anharmonic LD equations [Eqs. (15) and (16)] include only first- and second-order perturbations. We note that if we use a constant value for ϵ (as done by others[22,23]) instead of our iterative procedure [see Eqs. (24)–(26)], the frequency shifts and linewidths calculated with anharmonic LD are in poor qualitative agreement with those computed with MD, particularly at the higher temperatures.

In Table II we tabulate the RMS frequency shift and linewidth normalized by the quasiharmonic frequencies over the entire Brillouin zone, $\langle (\Delta/\omega)^2 \rangle^{1/2}$ and $\langle (\Gamma/\omega)^2 \rangle^{1/2}$. At a temperature of 20 K, the normalized anharmonic frequency shifts, as calculated with the BTE-LD and BTE-MD methods, are in reasonable agreement with each other. The linewidths calculated with the two methods are also in agreement. At this temperature, these anharmonic corrections are small compared to the quasiharmonic frequencies, but grow with increasing temperature. Above a temperature of 50 K, the anharmonic corrections become significant compared to the quasiharmonic frequencies and the BTE-based methods may no longer be accurate. At all temperatures considered, the linewidths predicted in the BTE-MD method are larger than those predicted in the BTE-LD method. This result is expected since fifth- and higher-order anharmonic terms are neglected in the BTE-LD method but not in the BTE-MD method.

V. PREDICTION RESULTS

A. Thermal-conductivity predictions

The predicted thermal conductivities from the four methods are plotted against temperature in Fig. 3 and listed in Table III. Unlike the BTE-LD and BTE-MD prediction methods, there are no major assumptions inherent to the GK-MD and direct-MD methods other than the choice of the interatomic potential, which is consistent here. We thus take

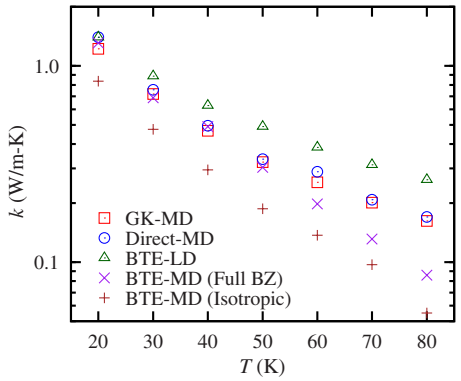

FIG. 3. (Color online) Temperature dependence of the thermal conductivity predicted from the four methods. Using an isotropic approximation (isotropic) rather than all the phonons in the full Brillouin zone (full BZ) in the BTE-MD method causes the thermal conductivity to be underpredicted by a factor of about 1.5.

the GK-MD and direct-MD thermal-conductivity predictions to be the most accurate and use them to assess the range of applicability of the BTE-LD and BTE-MD methods. The predicted thermal-conductivity values from the GK-MD and direct-MD methods are in good agreement, generally within 10% (except at temperatures of 20 and 60 K where the predictions are within 15%). Others have also found that GK-MD and direct-MD thermal-conductivity predictions are consistent.[35,36] The thermal conductivities predicted with the BTE-LD and BTE-MD methods are within 15% of both the GK-MD and direct-MD values at a temperature of 20 K. As the temperature increases, the BTE-MD method begins to underpredict the thermal conductivity by an increasing amount. This loss of accuracy is due to error introduced by mapping the atomic positions and velocities onto the quasiharmonic normal-mode coordinates, which become less representative of the real system as the temperature increases. As the temperature increases above 20 K, the BTE-LD method begins to overpredict the thermal conductivity by an increasing amount. This overprediction can be attributed to the exclusion of higher-order phonon processes resulting in reduced anharmonicity of the argon crystal (see Fig. 2). The BTE-LD thermal-conductivity value at a temperature of 40 K is about 30% higher than the GK-MD and direct-MD predictions.

The thermal-conductivity predictions using the BTE-LD method with the quantum-mechanical expressions for the phonon distribution, specific heats, frequency shifts, and linewidth are also given in Table III. While not shown here, the full quantum-mechanical treatment correctly captures the expected thermal-conductivity trends at very low temperatures, including the experimentally observed maximum in the thermal conductivity and the decrease to zero at zero temperature. These low-temperature predictions cannot be made using MD because it is a classical method. As expected, above the maximum in the thermal conductivity, the quantum predictions closely agree with the classical BTE-LD predictions. Our quantum BTE-LD thermal-conductivity results agree to within 15% of the BTE-based quantum predictions made by Omini and Sparavigna[25] for argon at temperatures of 20 K (1.66 W/m-K) and 80 K (0.236 W/m-K).

TABLE III. Thermal-conductivity values in W/m-K from the four prediction methods. The BTE-LD values computed using the quantum expressions for the occupation number and specific heat are included for reference.

T (K)	GK-MD[a]	Direct-MD	BTE-MD	BTE-LD	Quantum BTE-LD
20	1.2	1.4	1.3	1.4	1.5
30	0.72	0.76	0.69	0.89	0.93
40	0.47	0.50	0.49	0.63	0.66
50	0.32	0.34	0.30	0.49	0.51
60	0.26	0.29	0.20	0.38	0.40
70	0.20	0.21	0.13	0.31	0.32
80	0.16	0.17	0.086	0.26	0.27

[a]Reference 16.

Based on the thermal-conductivity results in this section and the analysis in Sec. IV D, we suggest that, for LJ argon, reasonable quantitative predictions of the thermal conductivity can be made up to half the Debye temperature (40 K) with the BTE-LD method and up to 70% of the Debye temperature with the BTE-MD method. Based on these thermal-conductivity results and our BTE-LD thermal-conductivity predictions of Stillinger-Weber silicon,[37] we propose that, as a general rule, the BTE-LD predictions are accurate up to one-half of the Debye temperature.

B. Mode-dependent thermal conductivity

Using the BTE-MD method and an isotropic approximation (similar to the method described by McGaughey and Kaviany[14] and Henry and Chen[31]), we predict thermal conductivities for LJ argon that are about a factor of 1.5 lower than our predictions using the full Brillouin zone (see Fig. 3). This discrepancy is a result of the inaccuracy of the isotropic approximation for LJ argon. An examination of the phonon properties for the entire Brillouin zone from our BTE-LD and BTE-MD calculations reveals that the relaxation times can be treated isotropically (i.e., as a function of only frequency and temperature). We find, however, that the distribution of phonons and the group velocities in the [100] direction are not representative of the entire Brillouin zone.

Using the phonon information obtained from the BTE-LD method, we plot, in Fig. 4, the contribution to the thermal conductivity as a function of $\omega_A/(\omega_A)_{\max}$, the phonon frequency divided by the maximum phonon frequency. For this classical system, temperature changes the maximum frequency but has no effect on the curves in Fig. 4. The largest contribution to the thermal conductivity comes from the phonons around half of the maximum frequency. This large contribution is due to the large number of phonons near that frequency (see the density-of-states curve in Fig. 4). Dividing the thermal-conductivity contribution by the density of states gives the average contribution per mode ($c_{ph}v_{g,x}^2\tau$) as a function of frequency ratio. We see that, on average, each low-frequency mode contributes much more than individual phonons at the higher frequencies (the downturn near zero frequency is due to the finite number of unit cells considered). This fact helps to explain why we need to correct for the missing states around the zone center and is what leads to a common assumption that low-frequency phonons dominate thermal transport. This assumption is clearly not valid for LJ argon.

C. Computational cost

The computational cost of each of the prediction methods is a major concern. For the test argon system, the GK-MD and direct-MD prediction methods require similar computational resources ($\approx$10–20 processor hours for each temperature). The computation time required for the BTE-LD method is an order of magnitude less ($\approx$1 processor hour for each temperature) while the BTE-MD method is extremely demanding ($\approx$25 processor days for each temperature). Efficient MD codes scale linearly with the number of atoms in the computational domain; thus, so do the GK-MD and direct-MD methods. The BTE-MD method scales as the square of the number of atoms $[(Nn)^2]$. The computational cost of the BTE-LD method is proportional to N^2n^4. This poor scaling makes the BTE-LD method computationally expensive for materials with a large number of atoms in the unit cell.

For the BTE-LD method, it is possible to make several approximations that will reduce the computational cost re-

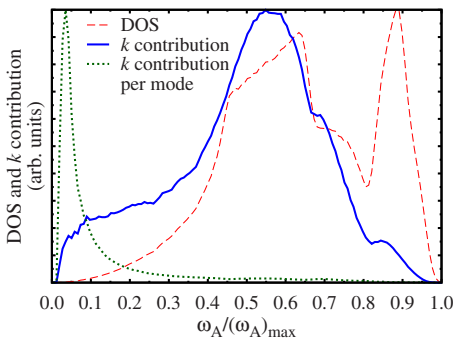

FIG. 4. (Color online) Dependence of the thermal conductivity and phonon density of states (DOS) on $\omega_A/(\omega_A)_{\max}$ at a temperature of 50 K.

quired without sacrificing much accuracy. We used one such approximation when we neglected interactions beyond nearest neighbors in the anharmonic LD calculations. Other possible approximations include neglecting high-frequency phonons, which make little contribution to the thermal conductivity, (i.e., do not calculate Δ or Γ for frequencies greater than some cutoff), or by using a single coarse wave-vector grid to compute the thermal conductivity (i.e., do not perform the extrapolation). Using a $6\times6\times6$ grid of wave vectors gives thermal-conductivity values that are at most 15% lower than the extrapolated values but with 2% of the computational cost ($\approx$1.5 minutes).

VI. CONCLUSIONS

The BTE-LD and BTE-MD methods for predicting the phonon properties and thermal conductivity of a crystal have been presented, including unique solutions to several challenges inherent to these methods. The thermal-conductivity predictions made with the BTE-based methods were then compared to predictions made using the GK-MD and direct-MD methods. All of the prediction methods give thermal-conductivity values for LJ argon that agree at low temperature (20 K). As the temperature is increased, the BTE-LD and BTE-MD predictions diverge from the GK-MD and direct-MD predictions (see Fig. 3) due to reduced validity of the low-temperature approximations made in the LD calculations. By analyzing the phonon velocities, frequencies, and lifetimes, we find that the isotropic approximation is invalid for argon. We also find that on a per mode basis the low-frequency phonons contribute the most to the thermal conductivity. However, as shown in Fig. 4, by considering the phonon density of states, phonons with a frequency of half the maximum frequency are found to dominate thermal transport. Such information will be valuable in designing nanostructures with tailored thermal properties. For example, to increase the figure of merit of a thermoelectric material, the size and number of nanoparticles in a crystal could be altered to selectively scatter the dominant phonon modes, reducing the thermal conductivity while maintaining the electrical transport properties.[7–9]

By considering the root-mean-square displacements, frequency shifts, and linewidths, we suggest that the LD calculations for LJ argon are reasonably accurate up to a temperature of 50 K (see Sec. IV D). At this temperature, we find the BTE-MD predicted thermal-conductivity value to be about 10% lower than the GK-MD and direct-MD values. For the BTE-LD method, neglecting fifth- and higher-order potential-energy terms causes the thermal-conductivity predictions to become inaccurate above a temperature of 40 K. At this temperature, the BTE-LD thermal-conductivity prediction is about 30% higher than the GK-MD and direct-MD predictions. For other insulators and semiconductors, we suggest that half the Debye temperature is the maximum temperature at which the BTE-LD method provides accurate thermal-conductivity predictions, while the BTE-MD method is accurate up to 70% of the Debye temperature. Above these temperatures the approximations made in the BTE-based methods become inaccurate, and the GK-MD and direct-MD prediction methods are more appropriate to use.

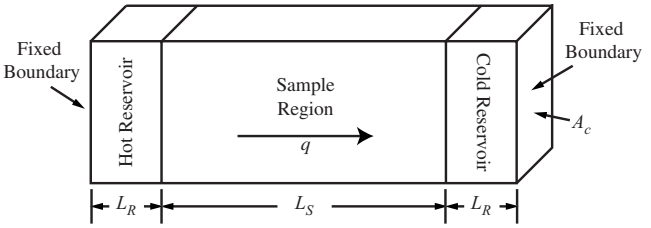

FIG. 5. Schematic of the simulation cell used in the direct method.

We note that for our thermal-conductivity predictions the BTE-LD method requires an order of magnitude less computing effort than the GK-MD and direct-MD methods. Additionally, several approximations can be made within the LD framework that allow the thermal conductivity to be estimated using the BTE-LD method in a matter of minutes. For designing materials with tailored thermal transport properties, the ability to rapidly estimate the thermal conductivity will be a useful way to screen for promising designs that deserve more in-depth study.

Finally, we note that the BTE-LD method is amenable to making highly accurate predictions of the thermal conductivity that can be directly compared to experiment. For our predictions, we used the LJ interatomic potential to compute the force constants (second-, third-, and fourth-order energy derivatives) required for the LD calculations. These force constants can be obtained from other sources. For example, Broido *et al.*[29] used density-functional perturbation-theory calculations to provide input for harmonic LD calculations and calculations of phonon-phonon-scattering probabilities [related to Eq. (16)]. These probabilities were then used in the BTE to obtain thermal-conductivity predictions for silicon and germanium that are in excellent agreement with experiment. Such an approach could also be used in the BTE-LD method discussed here.

ACKNOWLEDGMENTS

This work is supported in part by the Pennsylvania Infrastructure Technology Alliance, a partnership of Carnegie Mellon, Lehigh University, and the Commonwealth of Pennsylvania's Department of Community and Economic Development (DCED). Additional support is provided by Advanced Micro Devices (AMD) and the Berkman Faculty Development Fund at Carnegie Mellon University.

APPENDIX: DIRECT-MD METHOD

The direct-MD method is a nonequilibrium steady-state approach based on the Fourier law, Eq. (1).[35,36,38] The thermal conductivity is found by imposing a heat flux across the sample and measuring the resulting temperature gradient. A schematic of the direct method simulation cell is shown in Fig. 5. The system consists of a sample bordered by hot and cold reservoirs and fixed boundaries in the direction parallel to the applied heat flux. Periodic boundary conditions are

imposed in the directions perpendicular to the heat flux.

For our argon system, the fixed boundary regions each contain four layers of fixed atoms in order to prevent the sublimation of the reservoir atoms. The thermal conductivity is found to be independent of the reservoir length, L_R, when L_R is greater than or equal to four atomic layers. The predicted thermal conductivity is independent of the system dimensions in the directions perpendicular to the applied heat flux when they are greater than or equal to four conventional unit cells.

In the direct-MD method simulations, the system temperature is initially set to a uniform value by scaling the atomic velocities for 25 000 time steps. The heat flux is then generated using the method described by Ikeshoji and Hafskjold.[39] From the point when the heat flux is first applied, a period of one million time steps is allowed for the sample to reach steady state. The temperature of each atomic layer is then averaged over an additional two million time steps. The temperature gradient is calculated using a least-squares regression analysis fit to the temperature profile. The ten atomic layers closest to each reservoir are neglected when specifying the temperature gradient because the temperature profile in these regions is nonlinear due to phonon scattering at the reservoir/sample interfaces. This nonlinear effect is most pronounced at the lower temperatures.

The thermal conductivity predicted by the direct method can be dependent on the sample length, L_s, if L_s is not much greater than the bulk phonon mean-free path. For example, when L_s is on the order of or less than the bulk phonon mean-free path, the amount of phonon scattering at the boundaries between the reservoirs and the sample is comparable to that occurring within the sample itself. Furthermore, phonons can potentially travel from the hot reservoir to the cold reservoir without scattering (i.e., ballistic transport). Both of these effects lead to a dependence between the thermal conductivity and L_s.

We find that the sample length effect is negligible for $T \geq 50$ K when L_s is greater than or equal to 160 atomic layers. For $T \leq 40$ K, however, the thermal conductivity is still dependent on L_s even for $L_s = 200$ atomic layers. For these low temperatures, we extrapolate the results from simulations with sample lengths of 114, 132, 160, and 200 atomic layers to obtain the thermal conductivity of an infinite system using the method described by Schelling *et al.*[35]

*Corresponding author: mcgaughey@cmu.edu

[1] *Thermal Conductivity Theory, Properties, and Applications, Physics of Solids and Liquids*, edited by T. M. Tritt (Kluwer Acedemic/Plenum Publishers, New York, 2004).
[2] W. Liu and M. Asheghi, ASME J. Heat Transfer **128**, 75 (2006).
[3] T. Borca-Tasciuc, W. Liu, J. Liu, T. Zeng, D. Song, C. Moore, G. Chen, K. Wang, and M. Goorsky, Superlattices Microstruct. **28**, 199 (2000).
[4] S. Chakraborty, C. A. Kleint, A. Heinrich, C. M. Schneider, J. Schumann, M. Falke, and S. Teichert, Appl. Phys. Lett. **83**, 4184 (2003).
[5] D. G. Cahill, W. K. Ford, K. E. Goodson, G. D. Mahan, A. Majumdar, H. J. Maris, R. Merlin, and S. R. Phillpot, J. Appl. Phys. **93**, 793 (2003).
[6] C. J. Gomes, M. Madrid, J. V. Goicochea, and C. H. Amon, ASME J. Heat Transfer **128**, 1114 (2006).
[7] W. Kim, J. Zide, A. Gossard, D. Klenov, S. Stemmer, A. Shakouri, and A. Majumdar, Phys. Rev. Lett. **96**, 045901 (2006).
[8] W. Kim, S. L. Singer, and A. Majumdar, J. Phys.: Conf. Ser. **92**, 012085 (2007).
[9] N. Mingo, D. Hauser, N. P. Kobayashi, M. Plissonnier, and A. Shakouri, Nano Lett. (to be published).
[10] *CRC Handbook of Chemistry and Physics*, 88th ed., edited by D. R. Lide (CRC, Boca Raton, FL, 2008).
[11] N. W. Ashcroft and N. D. Mermin, *Solid State Physics* (Saunders College Publishing, Fort Worth, 1976).
[12] J. Lukes, D. Li, X.-G. Liang, and C.-L. Tien, ASME J. Heat Transfer **122**, 536 (2000).
[13] A. J. H. McGaughey and M. Kaviany, Int. J. Heat Mass Transfer **47**, 1783 (2004a).
[14] A. J. H. McGaughey and M. Kaviany, Phys. Rev. B **69**, 094303 (2004b).
[15] H. Kaburaki, J. Li, S. Yip, and H. Kimizuka, J. Appl. Phys. **102**, 043514 (2007).
[16] A. J. H. McGaughey, Ph.D. thesis, University of Michigan, 2004.
[17] G. P. Srivastava, *The Physics of Phonons* (Adam Hilger, Bristol, 1990).
[18] J. M. Ziman, *Electrons and Phonons: The Theory of Transport Phenomena in Solids* (Clarendon, Oxford, 1960).
[19] M. T. Dove, *Introduction to Lattice Dynamics* (Cambridge University Press, Cambridge, UK, 1993).
[20] A. J. H. McGaughey, M. I. Hussein, E. S. Landry, M. Kaviany, and G. M. Hulbert, Phys. Rev. B **74**, 104304 (2006).
[21] D. C. Wallace, *Thermodynamics of Crystals* (Wiley, New York, 1972).
[22] A. A. Maradudin and A. E. Fein, Phys. Rev. **128**, 2589 (1962).
[23] A. J. C. Ladd, B. Moran, and W. G. Hoover, Phys. Rev. B **34**, 5058 (1986).
[24] M. Omini and A. Sparavigna, Physica B **212**, 101 (1995).
[25] M. Omini and A. Sparavigna, Phys. Rev. B **53**, 9064 (1996).
[26] M. Omini and A. Sparavigna, Nuovo Cimento D **19**, 1537 (1997).
[27] D. A. Broido and T. L. Reinecke, Phys. Rev. B **70**, 081310(R) (2004).
[28] D. A. Broido, A. Ward, and N. Mingo, Phys. Rev. B **72**, 014308 (2005).
[29] D. A. Broido, M. Malorny, G. Birner, N. Mingo, and D. A. Stewart, Appl. Phys. Lett. **91**, 231922 (2007).
[30] In their paper, McGaughey and Kaviany incorrectly take the decay constant to be half the relaxation time. We divide their reported relaxation times by 2 to correct for the error.
[31] A. S. Henry and G. Chen, J. Comput. Theor. Nanosci. **5**, 1 (2008).
[32] J. Goicochea, M. Madrid, and C. Amon, Proc. ITHERM '06 (2006), p. 1185.
[33] A. Majumdar, in *Microscale Energy Transport*, edited by C.-L. Tien, A. Majumdar, and F. M. Gerner (Taylor and Francis,

Washington, 1998), p. 72.
[34] L. Kantorovich, *Quantum Theory of the Solid State: An Introduction*, Fundamental Theories of Physics, Vol. 136 (Kluwer, Dordrecht, 2004).
[35] P. K. Schelling, S. R. Phillpot, and P. Keblinski, Phys. Rev. B **65**, 144306 (2002).
[36] E. S. Landry, M. I. Hussein, and A. J. H. McGaughey, Phys. Rev. B **77**, 184302 (2008).
[37] J. E. Turney, E. S. Landry, A. J. H. McGaughey, and C. H. Amon (unpublished).
[38] A. J. H. McGaughey and M. Kaviany, in *Advances in Heat Transfer*, edited by G. Greene, Y. Cho, J. Hartnett, and A. Bar-Cohen (Elsevier, New York, 2006), Vol. 39, pp. 169–255.
[39] T. Ikeshoji and B. Hafskjold, Mol. Phys. **81**, 251 (1994).